Critical Opalescence and Its Impact on the Jet Quenching Parameter $\hat{q}$

Jing Wu(武警)[1], Shanshan Cao(曹杉杉)[2*], and Feng Li(李峰)[1,3,4,5*]

[1]*School of Physical Science and Technology, Lanzhou University, Lanzhou 730000, China*
[2]*Institute of Frontier and Interdisciplinary Science, Shandong University, Qingdao 266237, China*
[3]*Research Center for Hadron and CSR Physics, Lanzhou University and Institute of Modern Physics of CAS, Lanzhou 730000, China*
[4]*Lanzhou Center for Theoretical Physics, Key Laboratory of Theoretical Physics of Gansu Province, and Frontiers Science Center for Rare Isotopes, Lanzhou University, Lanzhou 730000, China*
[5]*Frontiers Science Center for Rare Isotopes, Lanzhou University, Lanzhou 730000, China*

(Received 24 January 2024; accepted manuscript online 13 March 2024)

Jet quenching parameter $\hat{q}$ is essential for characterizing the interaction strength between jet partons and nuclear matter. Based on the quark-meson model, we develop a new framework for calculating $\hat{q}$ at finite chemical potentials, in which $\hat{q}$ is related to the spectral function of the chiral order parameter. A mean field perturbative calculation up to the one-loop order indicates that the momentum broadening of jets is enhanced at both high temperature and high chemical potential, and approximately proportional to the parton number density in the partonic phase. We further investigate the behavior of $\hat{q}$ in the vicinity of the critical endpoint (CEP) by coupling our calculation with a recently developed equation of state that includes a CEP in the universality class of the Ising model, from which we discover the partonic critical opalescence, i.e., the divergence of scattering rate of jets and their momentum broadening at the CEP, contributed by scatterings via the σ exchange process. Hence, for the first time, jet quenching is connected with the search of CEP.

DOI: 10.1088/0256-307X/41/3/031202

Imaging the QCD phase structure is one of the central goals of the high-energy nuclear collision programs at the Relativistic Heavy-Ion Collider (RHIC) and the Large Hadron Collider (LHC). It is now generally accepted that a strongly coupled quark-gluon plasma (QGP) is produced when heavy nuclei collide with ultra-relativistic energies, as revealed by the collectivity of soft hadron emission and the jet quenching phenomenon.[1,2] While the transition from the QGP to the hadronic matter is known to be a smooth crossover[3,4] at vanishing baryon chemical potential ($\mu_{\rm B}$), whether there exists a first order phase transition at large $\mu_{\rm B}$, and if so, where the critical endpoint (CEP) locates in the QCD phase diagram, are still open questions.

Extensive efforts have been devoted to seeking and locating CEP. It has been proposed that QCD criticality can be characterized by the high order cumulants of conserved quantities like baryon number.[5–8] Sophisticated dynamic model calculations[9–16] have been developed to explore signatures of CEP that survive the evolution of the complex system. Experimentally, a deviation of the ratio between the fourth and second cumulants of the net proton number from unity at certain $\sqrt{s_{\rm NN}}$, plausibly caused by criticality, has been suggested by the Beam Energy Scan (BES) program at RHIC,[17] which waits for confirmation with more precise data soon. Meanwhile, the amplification of the light nuclei multiplicity ratio is recently proposed as an alternative signal of CEP.[18]

Besides the above observables, jets have served as a successful tool in discovering and probing the QGP. Recent experimental and theoretical advances broaden jet studies from medium modification on jets[19–22] to jet-induced medium excitations,[23,24] allowing one to explore jet–medium interactions with jet-correlated soft hadrons, e.g., jet substructures,[25–33] γ/Z-triggered hadron distributions[33–37] and hadron chemistry within and around the jet cone.[38,39] However, rare discussions are available on utilizing jets to probe the QCD phase diagram. Unlike soft hadrons and light nuclei that carry information at either chemical or kinetic freeze-out, energetic jets interact locally with the QGP, thus encode direct information on the phase boundary and could be a more advanced probe of the critical behavior. In fact, the nuclear modification of hard hadrons has already been measured in the BES program,[40] which shows a hint of additional suppression at certain centrality in Au+Au collisions at 14.5 AGeV, but has been overlooked for years.

Jet evolution can be characterized by the jet quenching parameter $\hat{q}$[41,42] that measures its transverse momentum broadening square per unit time. Evaluating $\hat{q}$ from the first-principle method[43–45] or extracting it from the jet data[22,46–48] are ongoing efforts at the frontier of heavy-ion physics. In this work, we use two methods to calculate the jet parameters at finite temperature and chemical potential. Using a quark-meson (QM) model[49] possessing a chiral phase transition, we calculate $\hat{q}$ at finite $\mu_{\rm B}$ up to the one-loop order. This calculation is further coupled with

*Corresponding authors. Email: shanshan.cao@sdu.edu.cn; fengli@lzu.edu.cn
© 2024 Chinese Physical Society and IOP Publishing Ltd

an equation of state incorporating a CEP in the universality class of the Ising model,[50,51] from which a prominent enhancement around CEP is found for $\hat{q}$. Such an enhancement, named as *partonic critical opalescence* (PCO) in analogy to the normal critical opalescence, might lead to the additional suppression of the hard hadron yield mentioned above, thus providing a new method for exploring the QCD phase diagram around CEP.

Jet Quenching Parameter and Field–Field Correlation. We consider an approximately on-shell jet quark with momentum q scatters elastically with a medium (M) by exchanging momentum k. The color-isospin-spin averaged matrix element squared reads[43]

$$W(k) = \frac{1}{2N_c N_f}|\langle q+k; X|\mathcal{T}e^{-i\int_0^t dt' H_I(t')}|q; M\rangle|^2, \quad (1)$$

where t denotes the propagation time of the quark inside the medium, H_I is the interacting Hamiltonian in the interaction picture, X represents the final state of the medium, and $\mathcal{T}$ is the time ordering operator. Here, the initial and final states are assumed to be direct products of the medium and the free quark states, where the latter satisfies the box normalization condition, $q(x)|q\rangle = e^{iqx}u(q)/\sqrt{2E_qV}$ with $q(x)$ standing for the quark field and $u(q)$ denoting the Dirac spinor. The initial and final jet quark momenta are assumed light-like, i.e., $q^2 = (q+k)^2 = 0$. The jet quenching parameter and the scattering rate can then be obtained as

$$\hat{q} \equiv \frac{\langle \boldsymbol{k}_\perp^2\rangle}{t} = \sum_{k,X} \boldsymbol{k}_\perp^2 \frac{W(k)}{t}. \quad (2)$$

In this work, the jet–medium interaction is described using the QM model,[49] where interactions among quarks are mediated by the mesonic fields, such as σ and π, rather than gluons. In the hadronic phase, these fields can be directly viewed as σ and π particles, while in the QGP phase, they are only effective descriptions of the force mediator. The QM model is widely employed as a possible imitation of QCD at finite chemical potentials with a chiral phase transition and a corresponding CEP embedded. Although the applicability of the QM model at very high temperature might be questionable, we consider it as a reasonable description around the phase transition boundary, especially when exploring the behavior of $\hat{q}$ near the CEP, as it reproduces the equation of state obtained by lattice QCD up to twice of the pseudo-critical temperature at vanishing baryon chemical potential.[49] The full Lagrangian of the QM model will be given in the next section, while its interaction sector is

$$H_I = g\int d^3x \bar{q}(\sigma' + i\gamma_5 \vec{\pi}\cdot\vec{\tau})q, \quad (3)$$

where τ denotes the Pauli matrix, and σ' is the fluctuation of the σ field around its expectation value σ^* given by the gap equation.[49]

After expanding Eq. (1) in terms of H_I and keeping only the leading order, one obtains $\hat{q} = \hat{q}_\sigma + \hat{q}_\pi$ with

$$\hat{q}_{\sigma/\pi} = \frac{g^2}{(2\pi)^3 N_c N_f}\int \frac{d^3\boldsymbol{k}}{E_q E_{q+k}} k_\perp^2 q\cdot(q+k)\tilde{G}_{\sigma/\pi}(k), \quad (4)$$

in which

$$\widetilde{G}_\sigma(k) = \int d^4x\langle M|\sigma'(0)\sigma'(x)|M\rangle e^{ik\cdot x},$$
$$\widetilde{G}_\pi(k) = \int d^4x\langle M|\vec{\pi}(0)\cdot\vec{\pi}(x)|M\rangle e^{ik\cdot x} \quad (5)$$

represent the correlation functions of σ and π fields between different locations. The physical significance of the σ field in the QM model is the quark condensate, which is considered as the order parameter of the chiral phase transition. Therefore, via Eq. (4), we connect the jet quenching parameter $\hat{q}$ with the correlation function of the order parameter, and hence the correlation length that diverges at CEP.

The correlation functions can be further expressed using the spectral functions ($\widetilde{\rho}_{\sigma/\pi}$) via the Kubo–Martin–Schwinger relation[52,53]

$$\widetilde{G}_{\sigma/\pi}(k) = \frac{d_{\sigma/\pi}}{e^{\beta k_0}-1}\widetilde{\rho}_{\sigma/\pi}(k), \quad (6)$$

with $d_\sigma = 1$ and $d_\pi = 3$ representing the degeneracy of the σ and π fields respectively.

Jet Quenching Parameter at Finite Chemical Potential. The spectral function in Eq. (6) is evaluated perturbatively within the QM model whose Lagrangian is

$$\mathcal{L} = \bar{q}[i\partial\cdot\gamma - g(\sigma + i\gamma_5\vec{\pi}\cdot\vec{\tau})]q + \frac{1}{2}(\partial_\mu\sigma)^2 + \frac{1}{2}(\partial_\mu\vec{\pi})^2 - \Big[\frac{\lambda}{4}(\sigma^2+\vec{\pi}^2-v^2)^2 - c\sigma\Big], \quad (7)$$

where c is the explicit symmetry breaking parameter and λ is the quartic coupling constant. The parameters are determined by fitting the vacuum π and σ masses and the pion decay constant as $g = 3.2$, $c = 1.77\times10^6\,\mathrm{MeV}^3$, $\lambda = 19.7$, and $v = 87.6\,\mathrm{MeV}$.[49] With this setup, the CEP is obtained from solving $(\partial p/\partial n_B)_T = (\partial^2 p/\partial n_B^2)_T = 0$ under the mean-field approximation as $T_c \approx 89\,\mathrm{MeV}$ and $n_B \approx 0.21\,\mathrm{fm}^{-3}$ (or $\mu_c \approx 228\,\mathrm{MeV}$). Thanks to the presence of the explicit symmetry breaking term ($c\sigma$), the σ field is of a non-vanishing expectation value which should be evaluated by minimizing the thermodynamic potential (or solving the gap equation equivalently).[49] Therefore, the σ field can be decomposed as $\sigma = \sigma^* + \sigma'$, where the space-time independent expectation value σ^* contributes to the effective mass of the medium quark as $M_q = g\sigma^*$, while the fluctuating sector σ' carries the dynamics of the σ field. Hence, the spectral function of the σ field actually describes the excitation property of σ'.

The spectral functions of σ and π fields in the QM model can be generally expressed as

$$\widetilde{\rho}_{\sigma/\boldsymbol{\pi}}(k) = 2\mathrm{Im}\frac{1}{-k_*^2 + m_{\sigma/\pi}^2 + g^2\Pi_{\sigma/\pi}(k_*)}, \quad (8)$$

where $k_* \equiv (k^0 + i0^+, \boldsymbol{k})$, $m_\sigma^2 = \lambda(3\sigma^{*2} - v^2)$ and $m_\pi^2 = \lambda(\sigma^{*2} - v^2)$ are the vacuum masses of the σ/π fields, and

$$\Pi_\sigma(i\omega_n, \boldsymbol{k}) = \int_0^\beta d^4x\,\mathrm{tr}[S(x)S(-x)]e^{i(\omega_n t - \boldsymbol{k}\cdot\boldsymbol{x})},$$
$$\Pi_\pi(i\omega_n, \boldsymbol{k}) = -\int_0^\beta d^4x\,\mathrm{tr}[S(x)\gamma_5 S(-x)\gamma_5]e^{i(\omega_n t - \boldsymbol{k}\cdot\boldsymbol{x})} \quad (9)$$

are the self energies of σ/π evaluated up to one fermion loop, with

$$\widetilde{S}(i\nu_n, \boldsymbol{p}) = \frac{(i\nu_n - \mu)\gamma_0 - \boldsymbol{\gamma}\cdot\boldsymbol{p} - M_q}{(i\nu_n - \mu)^2 - \boldsymbol{p}^2 - M_q^2} \tag{10}$$

representing the Matsubara propagator of the medium quark. Although the frequencies $i\omega_n \equiv 2\pi i n T$, $i\nu_n \equiv i\pi(2n+1)T$ in Eqs. (9) and (10) are imaginary and discrete, an analytical continuation $i\omega_n \to k^0 + i0^+$ is applied when evaluating the self energies in Eq. (8).

Shown in the upper panels of Fig. 1 are the spectral functions of σ (left) and π (right) fields at $\boldsymbol{k} = 0$. Those obtained at CEP, in the hadronic (or chiral symmetry breaking) phase and in the QGP (or the chiral symmetry restored) phase are plotted by the solid, dashed and dotted curves, respectively. It should be remarked that the σ effective mass, approximately indicated by the peak location of ρ_σ at $\boldsymbol{k} = 0$, first decreases and then increases as the temperature or the chemical potential increases, and achieves its minimum value at CEP (or on the phase boundary), while the π effective mass keeps growing with temperature and chemical potential. Meanwhile, the spectral functions of σ and π fields are almost degenerate in the QGP phase, which is regarded as one feature of chiral symmetry restoration.

The spectral functions at finite momentum transfer ($|\boldsymbol{k}| = 0.4\,\text{GeV}$) are presented in the lower panels of Fig. 1. Besides the similar peak structures shown in the region of $k^0 > |\boldsymbol{k}|$, additional bumps appear at $k^0 < |\boldsymbol{k}|$. Since the momentum transfer carried by the mesonic fields is spacelike in elastic scatterings, the jet quenching parameter $\hat{q}$ is directly contributed by these bumps. Furthermore, these bumps are drastically suppressed in the hadronic phase, suggesting an almost vanishing $\hat{q}$ in the hadronic matter.

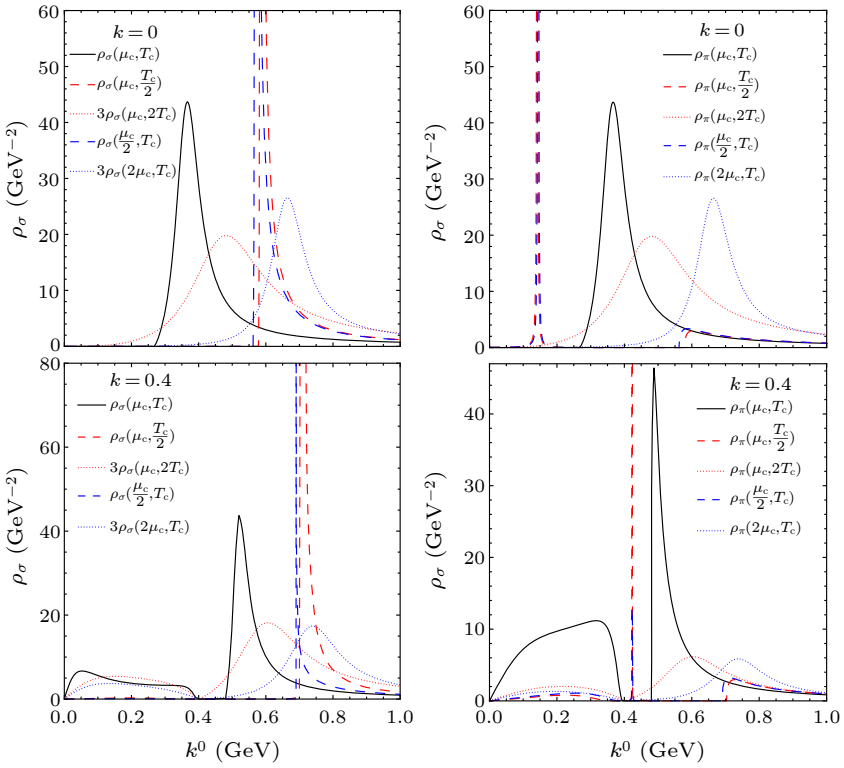

Fig. 1. The spectral functions of σ (left column) and π (right column) fields at various temperatures and chemical potentials with $\boldsymbol{k} = 0$ (upper row) and $|\boldsymbol{k}| = 0.4$ GeV (lower row), evaluated perturbatively up to the one-loop level.

By substituting the spectral functions of Eq. (8) into Eq. (6) and then Eq. (4), we obtain the jet quenching parameter contributed by the σ and π exchange processes, as shown in the left and right panels of Fig. 2, respectively. It is illustrated that $\hat{q}_{\sigma/\pi}$ almost vanishes in the chiral symmetry breaking phase and grows with not only temperature but also chemical potential. In addition, we find that $\hat{q}$ is approximately proportional to the parton number density n_{parton}, which is the summation of the quark and anti-quark number density in the QM model, in the chiral symmetry restored phase. This is consistent with the empirical scenario that the scattering rate of a jet parton is proportional to the density of scattering centers inside the QGP, as suggested by perturbative QCD calculations.[22] To further investigate the dimensionless ratio $\hat{q}/n_{\text{parton}}$, we plot them on the phase diagram in Fig. 3 for the σ and π exchange processes respectively. It shows that quantitatively, $\hat{q}_\sigma \sim (0.22 \pm 0.03) n_{\text{parton}}$, $\hat{q}_\pi \sim (0.65 \pm 0.1) n_{\text{parton}}$, and thus $\hat{q} \sim (0.87 \pm 0.13) n_{\text{parton}}$ at high temperatures and chemical potentials. Both ratios are enhanced near the phase boundary, especially close to the first-order phase boundary, consistent with the behavior of $\hat{q}/T^3$ extracted for vanishing μ_{B} using the Bayesian analysis.[46–48] However, no special behavior of $\hat{q}$ is observed around CEP in

either Fig. 2 or Fig. 3. We shall see in the next section that it might be due to the unrealistic CEP obtained under the mean field approach.

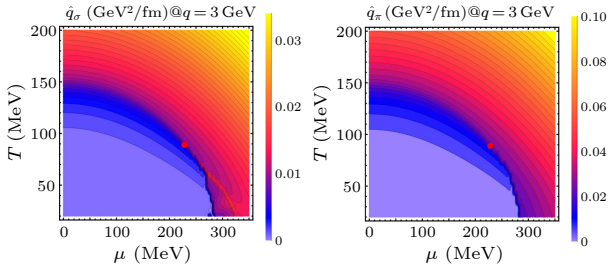

Fig. 2. Contour plots of the temperature and chemical potential dependent jet quenching parameter $\hat{q}$ for a jet quark at 3 GeV energy, contributed by the σ (left panel) and π (right panel) exchange processes. The CEP is labeled by the red dot.

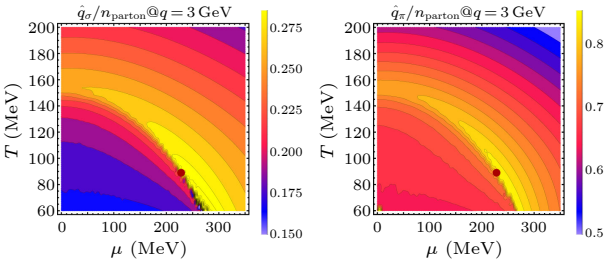

Fig. 3. Same as Fig. 2, except that $\hat{q}$ is rescaled by the parton number density $n_{\rm parton}$. The CEP is labeled by the dark red dot.

Jet Quenching Parameter near CEP. The universality of critical behaviors allows one to construct mappings among systems in the same class, hence transfers unknown spectral functions, e.g., those of the quark condensate in QCD, into well-established ones, e.g., those of the order parameter in the Ising model, near CEP. This has recently been developed for dealing with the freezing out procedure near the CEP [16] and implemented to study the critical behavior of the bulk viscosity,[50,51] and is now employed for investigating $\hat{q}$ here, and introduced briefly as follows.

Mapping between QCD and Ising Model. Here we shall denote the densities of the extensive thermodynamic variables of QCD and Ising model as $x^a \equiv (e, n)$ and $x^A \equiv (\epsilon, \psi)$ respectively, where e and n represent the energy and the baryon number densities of the QCD, ϵ and ψ represent the energy density and the spin density (the order parameter) of the Ising model, respectively. The mapping between x^a and x^A is not unique,[54] and is usually taken linear in literature [50,51,55] as

$$\begin{bmatrix}\delta e\\ \delta n\end{bmatrix} = \begin{bmatrix}M_{11} & M_{12}\\ M_{21} & M_{22}\end{bmatrix}\begin{bmatrix}\delta\epsilon\\ \delta\psi\end{bmatrix}, \tag{11}$$

where δ represents the variation from the critical value.

The mapping between the thermal conjugated variables, defined as $X_{A/a} \equiv -\partial S/\partial x^{A/a}$ with S being the entropy, is considered linear as well, where $X^a = (-\beta, \beta\mu)$ for QCD, and $X^A = (-\beta^{\rm Is}, \beta^{\rm Is}H)$ for the Ising model, with β and H representing the inverse temperature and the magnetic field respectively. In detail, it is expressed in Refs. [50,51,55] as

$$\begin{bmatrix}-\delta\beta\\ \delta(\beta\mu)\end{bmatrix} = \begin{bmatrix}\bar{M}_{11} & \bar{M}_{12}\\ \bar{M}_{21} & \bar{M}_{22}\end{bmatrix}\begin{bmatrix}-\delta\beta_{\rm Is}\\ \delta(\beta_{\rm Is}H)\end{bmatrix}. \tag{12}$$

Equations (11) and (12) can be further simplified to

$$\begin{bmatrix}t\\ \bar{\mu}\end{bmatrix} = \begin{bmatrix}\bar{A}_{11} & \bar{A}_{12}\\ \bar{A}_{21} & \bar{A}_{22}\end{bmatrix}\begin{bmatrix}r\\ h\end{bmatrix},$$
$$\begin{bmatrix}\delta s\\ \delta n\end{bmatrix} = \begin{bmatrix}A_{11} & A_{12}\\ A_{21} & A_{22}\end{bmatrix}\begin{bmatrix}m\\ \delta\psi\end{bmatrix}, \tag{13}$$

where $t = \frac{T-T_{\rm c}}{T_{\rm c}}$ and $\bar{\mu} = \frac{\mu-\mu_{\rm c}}{T_{\rm c}}$ are the reduced temperature and chemical potential in QCD, while $r = \frac{T^{\rm Is}-T_{\rm c}^{\rm Is}}{T_{\rm c}^{\rm Is}}$ and $h = \frac{H}{T_{\rm c}^{\rm Is}}$ are the reduced temperature and magnetic field in the Ising model, respectively. In addition, $\delta s = \frac{1}{T_{\rm c}}\delta e - \frac{\mu_{\rm c}}{T_{\rm c}}\delta n$ is the variation of entropy density in QCD, and $m \equiv \delta\epsilon/T_{\rm c}^{\rm Is}$.

Universality requires that the singular parts of the entropy are identical for both QCD and the Ising model, which, as illustrated in Ref. [55], leads to the relation between the mapping matrices, i.e., $M \cdot \bar{M}^T = A \cdot \bar{A}^T = I$.

Furthermore, Eq. (13) should map the phase boundary of the Ising model, formulated as $r < 0$ and $h = 0$, to the phase boundary of QCD, formulated as $\bar{\mu} > 0$ and $t = t(\bar{\mu}) \approx k_{\rm s}\bar{\mu}$, where $k_{\rm s} < 0$ is the slope of the phase boundary near CEP, which constrains the elements in A and $\bar{A}$ matrices as $k_{\rm s}\bar{A}_{21} = \bar{A}_{11}$ and $-k_{\rm s}A_{12} = A_{22}$.

We further require the mapping to be conformal, which results in two more constraints: $-k_{\rm s}\bar{A}_{12} = \bar{A}_{22}$, and $k_{\rm s}A_{21} = A_{11}$. Finally, to be consistent with Ref. [51], we take $\bar{A}_{12} = 1$ and $\bar{A}_{21} = \frac{2}{3k_{\rm s}-1}$, and the transforming matrices are

$$\bar{A} = \begin{pmatrix}\frac{2k_{\rm s}}{3k_{\rm s}-1} & 1\\ \frac{2}{3k_{\rm s}-1} & -k_{\rm s}\end{pmatrix},\ A = \frac{3k_{\rm s}-1}{1+k_{\rm s}^2}\begin{pmatrix}\frac{k_{\rm s}}{2} & \frac{1}{3k_{\rm s}-1}\\ \frac{1}{2} & -\frac{k_{\rm s}}{3k_{\rm s}-1}\end{pmatrix}. \tag{14}$$

With the above mapping, we can express σ' near CEP as $\sigma' = J \cdot A \cdot \phi$, where $J \equiv ((\partial\sigma/\partial s)_n, (\partial\sigma/\partial n)_{\rm s})$ is a pair of the thermal derivatives evaluated at CEP, transforming σ' into a superposition of δs and δn, and $\phi \equiv (m, \delta\psi)$.

Hence, the correlation and spectral function, i.e., $\tilde{G}_\sigma$ and $\tilde{\rho}_\sigma$, in Eq. (4) can be expressed as

$$G_\sigma(x) \equiv \langle\sigma'(x)\sigma'(0)\rangle = J_l A_{li}\langle\phi_i'(x)\phi_j'(0)\rangle A_{kj}J_k,$$
$$\tilde{\rho}_\sigma = \frac{k^0}{T}\tilde{G}_\sigma, \tag{15}$$

where $\langle\phi_i'(x)\phi_j'(0)\rangle$ can be evaluated non-perturbatively using the extended Landau–Ginzburg–Wilson (LGW) model as illustrated in detail in the following.

Correlations between the Observables in the LGW Model. The LGW Hamiltonian with phonon [56] is

$$\mathcal{H} = \beta H = \int d^3\boldsymbol{x}\Big(\frac{1}{2}(\nabla\psi)^2 + \frac{1}{2}\tilde{t}\psi^2 + \frac{1}{4}u_0\psi^4 + \frac{1}{2C_0}m^2 + \gamma_0 m\psi^2\Big). \tag{16}$$

where m, ψ, and C_0 are the reduced energy density, order parameter, and heat capacity, respectively.

The bare couplings u_0, C_0, and γ_0 are corrected in the medium by the thermal loops. The corrected or dressed couplings obey the scaling laws near the CEP as $C \propto \xi^{\frac{\alpha}{\nu}}$, $\gamma \propto \xi^{\frac{2\beta-1}{\nu}}$, $\widetilde{u} \equiv u - 2\gamma^2 C \propto \xi^{2\eta-1}$, where ξ is the correlation length and α, β, δ, η, ν are the critical exponents whose values are taken from Ref. [57] as $\alpha = 0.11$, $\beta = 0.33$, $\delta = 4.78$, $\eta = 0.036$, $\nu = 0.63$.

The expectation values $\bar{\psi}$ and $\bar{m}$ are obtained by minimizing the Hamiltonian, i.e., $\frac{\delta\mathcal{H}}{\delta m}|_{m=\bar{m}} = \frac{\delta\mathcal{H}}{\delta\psi}|_{\psi=\bar{\psi}} = 0$. The detailed expression for $\bar{\psi}$ is given in Ref. [57] as $\bar{\psi} = M_0 R^\beta \theta$, where R and θ are the functions r and h whose expressions are given later in Eq. (26). Here $\bar{\psi}$ also obeys the scaling law near the CEP as $\bar{\psi} \propto \xi^{-\frac{\beta}{\nu}}$. Hence, like the σ field, ψ and m fields can also be decomposed as $\psi = \bar{\psi} + \psi'$ and $m = \bar{m} + m'$, with m' and ψ' representing fluctuations around their expectation values.

The static correlation functions between ψ' and m' are given non-perturbatively from the partition function as

$$\begin{aligned}\chi_m &\equiv \int d^3\boldsymbol{x}\langle m'(\boldsymbol{x})m'(\boldsymbol{0})\rangle e^{i\boldsymbol{k}\cdot\boldsymbol{x}} \\ &= C + (\gamma C)^2[4\bar{\psi}^2\chi_\psi + 4\bar{\psi}\chi_{\psi:\psi^2} + \chi_{\psi^2}], \\ \chi_{m:\psi} &\equiv \int d^3\boldsymbol{x}\langle m'(\boldsymbol{x})\psi'(\boldsymbol{0})\rangle e^{i\boldsymbol{k}\cdot\boldsymbol{x}} \\ &= -\gamma C[2\bar{\psi}^2\chi_\psi + \chi_{\psi:\psi^2}],\end{aligned} \tag{17}$$

where

$$\chi_\psi \equiv \int d^3\boldsymbol{x}\langle\psi'(\boldsymbol{x})\psi'(\boldsymbol{0})\rangle e^{i\boldsymbol{k}\cdot\boldsymbol{x}} = \frac{\xi_0^2(\xi/\xi_0)^{2-\eta}}{1+(|\boldsymbol{k}|\xi)^{2-\eta}} \tag{18}$$

is taken from Ref. [57] with $\xi_0 \approx 1.2/\sqrt[3]{5}\,\mathrm{fm}$, satisfying $s_0\xi_0^3 \approx 1$, and

$$\begin{aligned}\chi_{\psi^2} &\equiv \int d^3\boldsymbol{x}\langle\psi'^2(\boldsymbol{x})\psi'^2(\boldsymbol{0})\rangle e^{i\boldsymbol{k}\cdot\boldsymbol{x}} \\ &\approx 2\int\frac{d^3\boldsymbol{k}'}{(2\pi)^3}\chi_\psi(\boldsymbol{k}-\boldsymbol{k}')\chi_\psi(\boldsymbol{k}'), \\ \chi_{\psi:\psi^2} &\equiv \int d^3\boldsymbol{x}\langle\psi'(\boldsymbol{x})\psi'^2(\boldsymbol{0})\rangle e^{i\boldsymbol{k}\cdot\boldsymbol{x}} \approx -3\widetilde{u}\bar{\psi}\chi_\psi\chi_{\psi^2}\end{aligned} \tag{19}$$

are evaluated perturbatively.

It should be noted that the LGW Model is static, i.e., no time derivative, and hence no time evolution, is involved in Eq. (16). The dynamics of both the m and ψ fields are introduced manually in analogy to Brownian motion as

$$\begin{aligned}\partial_t m &= -\Gamma_m \circ \frac{\delta\mathcal{H}}{\delta m} + \eta_m, \\ \partial_t\psi &= -\Gamma_\psi \circ \frac{\delta\mathcal{H}}{\delta\psi} + \eta_\psi,\end{aligned} \tag{20}$$

which, after linearization and Fourier transformation, are simplified to

$$\widetilde{\Omega}\cdot\begin{bmatrix}\widetilde{m}' \\ \widetilde{\psi}'\end{bmatrix} \equiv \begin{bmatrix}-ik^0 + \frac{\widetilde{\Gamma_m}}{C} & 2\gamma\bar{\psi}\widetilde{\Gamma_m} \\ 2\gamma\bar{\psi}\widetilde{\Gamma_\psi} & -ik^0 + \frac{\widetilde{\Gamma_\psi}}{\chi_\psi}\end{bmatrix}\begin{bmatrix}\widetilde{m}' \\ \widetilde{\psi}'\end{bmatrix} = \begin{bmatrix}\widetilde{\eta}_m \\ \widetilde{\eta}_\psi\end{bmatrix}, \tag{21}$$

where $\Gamma_{m/\psi}$ and $\eta_{m/\psi}$ are the damping rates and random forces, respectively. Modeling the critical dynamics with Brownian motion can be justified using the projection operator method as demonstrated in Appendix 5B in Ref. [54] and has been utilized to study the critical behavior of bulk viscosity [51] and to extract the spectral function of the slow modes near CEP. [58,59]

The damping rates are taken from Refs. [60,61], with Γ_m given by model B describing the critical dynamics of conserved quantities and Γ_ψ given by model H with Kawasaki's approximation, [61] as follows:

$$\begin{aligned}\widetilde{\Gamma}_m &= \lambda_m|\boldsymbol{k}|^2, \qquad \frac{\widetilde{\Gamma_\psi}}{\chi_\psi} = \frac{2T_{\mathrm{ls}}}{3}\Big(\frac{\xi_0}{\xi}\Big)^3 K(|\boldsymbol{k}|\xi), \\ K(x) &= \frac{3}{4}[1 + x^2 + (x^3 - x^{-1})\arctan(x)],\end{aligned} \tag{22}$$

with $\lambda_m = 1\,\mathrm{GeV}^2$ chosen in this calculation.

The random forces η are of vanishing expectation values but non-vanishing correlation functions, formulated as $\langle\eta_i(x)\eta_j(y)\rangle = D_{ij}(\boldsymbol{x}-\boldsymbol{y})\delta(x^0-y^0)$, with i, j being m or ψ. D_{ij} is constrained by the fluctuation-dissipation theorem. In detail, the equal-time correlation functions are considered time independent, i.e., $\langle\phi_i'(t,\boldsymbol{x})\phi_j'(t,\boldsymbol{y})\rangle = \langle\phi_i'(t+\delta t,\boldsymbol{x})\phi_j'(t+\delta t,\boldsymbol{y})\rangle$, which, combined with the equations of motion Eq. (21), leads to

$$\begin{aligned}\widetilde{D}_{mm} &= 2\widetilde{\Gamma}_m\Big(\frac{\chi_m}{C} + 2\gamma\bar{\psi}\chi_{m:\psi}\Big), \\ \widetilde{D}_{m\psi} &= \widetilde{D}_{\psi m} \\ &= \frac{\widetilde{\Gamma}_\psi}{\chi_\psi}\chi_{m:\psi} + 2\gamma\bar{\psi}\widetilde{\Gamma}_\psi\chi_m + \widetilde{\Gamma}_m\Big(\frac{\chi_{m:\psi}}{C} + 2\gamma\bar{\psi}\chi_\psi\Big), \\ \widetilde{D}_{\psi\psi} &= 2\widetilde{\Gamma}_\psi + 4\gamma\bar{\psi}\widetilde{\Gamma}_\psi\chi_{m:\psi}.\end{aligned} \tag{23}$$

The correlations between the random forces would generate the correlations between the m and ψ fields according to Eq. (21) as

$$\widetilde{\langle\phi_i'\phi_j'\rangle} = (\widetilde{\Omega}^{-1}\cdot\widetilde{D}\cdot\widetilde{\Omega}^{\dagger-1})_{ij}. \tag{24}$$

Substituting the obtained $\widetilde{\langle\phi_i'\phi_j'\rangle}$ in Eq. (15) and then in Eq. (4), we finally obtain the jet quenching parameter near the CEP contributed by the σ exchange channel.

Numerical Results. To plot $\hat{q}_\sigma$ on the phase diagram, one need to know the t–$\bar{\mu}$ or r–h dependence of the correlation length ξ, which is given in Ref. [57] as

$$\xi \approx \xi_0 R^{-\nu}\sqrt{1 - \frac{5\theta^2}{18}}, \tag{25}$$

where R and θ are the re-organized thermal parameters expressed as

$$\begin{aligned}r &= R(1-\theta^2), \quad h = h_0 R^{\beta\delta}\tilde{h}(\theta), \\ \tilde{h}(\theta) &= \theta + h_1\theta^3 + h_2\theta^5.\end{aligned} \tag{26}$$

The parameters are taken from Ref. [57] as $h_0 = 0.394$, $h_1 = -0.76201$, and $h_2 = 0.00804$. Note that when R approaches 0, both r and h vanish, and the system approaches the CEP.

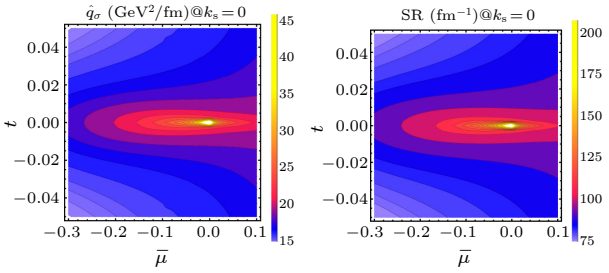

Fig. 4. The temperature and chemical potential dependencies of $\hat{q}_\sigma$ (left) and SR (right) near the CEP, with $k_s = 0$.

The jet quenching parameter $\hat{q}_\sigma$ and the corresponding scattering rate (SR), obtained by removing $k_\perp^2$ in the integration Eq. (4), with different values of k_s are plotted in Figs. 4 and 5. We see in both cases, $\hat{q}$ and SR are enhanced on the phase boundary and diverge at the CEP, which behave exactly like the classical critical opalescence.

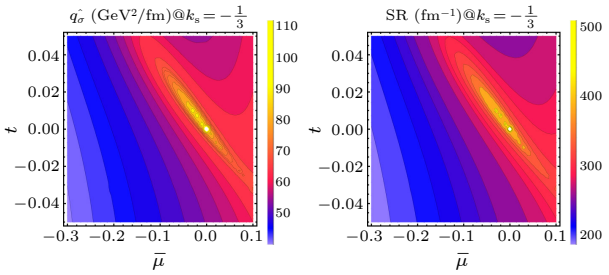

Fig. 5. The same as Fig. 4, except with $k_s = -\frac{1}{3}$.

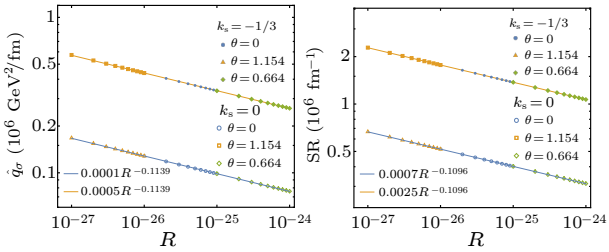

Fig. 6. The scale dependences of $\hat{q}$ (left) and SR (right) with respect to R for different k_s and θ when approaching the CEP.

For investigating the divergence in detail, we plot both $\hat{q}$ and SR within the extremely small R region with various θ and k_s in Fig. 6. In all these cases, $\hat{q}$ and SR exhibit the scaling behavior with almost the same critical exponent, i.e.,

$$\hat{q}_\sigma \sim SR_\sigma \sim R^{-0.11} \sim R^{-\alpha} = \xi^{\frac{\alpha}{\nu}}. \tag{27}$$

To better understand the scaling behavior of $\hat{q}$ and SR, one can look back into Eq. (4). Although it is an integration over $d^3\boldsymbol{k}$, due to the on-shell condition that $(q+k)^2 = 0$, it is actually an integration over $|\boldsymbol{k}|$ and k^0, i.e.,

$$\hat{q} \propto \int_0^\infty d|\boldsymbol{k}| \int_{|q-\boldsymbol{k}|-q}^{|\boldsymbol{k}|} dk^0 \cdots \widetilde{\langle \phi_i' \phi_j' \rangle}, \tag{28}$$

where $\cdots$ represents a non-singular function of $|\boldsymbol{k}|$ and k^0. On the other hand, when approaching the CEP,

$$\widetilde{\langle \phi_i' \phi_j' \rangle} \sim \begin{bmatrix} \frac{2\lambda_m |\boldsymbol{k}|^2 \xi^{\frac{2\alpha}{\nu}}}{\lambda_m^2 |\boldsymbol{k}|^4 + k_0^2 \xi^{\frac{2\alpha}{\nu}}} & 0 \\ 0 & \frac{\frac{T}{8\eta_0} \xi_0^\eta |\boldsymbol{k}|^{1+\eta}}{k_0^2 + (\frac{T}{16\eta_0})^2 |\boldsymbol{k}|^6} \end{bmatrix}, \tag{29}$$

where the off-diagonal terms are proportional to negative power of correlation length, and hence vanish near CEP. Notice that $\widetilde{\langle \phi_m' \phi_m' \rangle}$ peaks at $k^0 = 0$ and drops drastically when $|k^0| > \upsilon_{\boldsymbol{k}} \xi^{-\alpha/\nu}$, where $\upsilon_{\boldsymbol{k}}$ is an analytic function of $\boldsymbol{k}$. Therefore, the integration over k^0 can be estimated as

$$\begin{aligned} \hat{q} &\propto \cdots + \int_0^\infty d|\boldsymbol{k}| \int_{-\upsilon_{\boldsymbol{k}} \xi^{-\frac{\alpha}{\nu}}}^{\upsilon_{\boldsymbol{k}} \xi^{-\frac{\alpha}{\nu}}} dk^0 \cdots \widetilde{\langle \phi_m' \phi_m' \rangle} \\ &\propto \cdots + \int_0^\infty d|\boldsymbol{k}| \cdots \upsilon_{\boldsymbol{k}} \xi^{-\frac{\alpha}{\nu}} \widetilde{\langle \phi_m' \phi_m' \rangle}|_{k^0 \to 0} \propto \xi^{\frac{\alpha}{\nu}}, \end{aligned} \tag{30}$$

which is consistent with the numerical results shown in Fig. 6.

In short, similar to the classical critical opalescence where scatterings between the light and the medium are drastically enhanced, both the $\hat{q}$ and the scattering rate are found divergent at the CEP with the scaling rule $\hat{q} \propto SR \propto \xi^{\alpha/\nu}$. This also explains why we did not see special behavior around the CEP in the previous section within the QM model with the mean field approximation, since $\alpha = 0$ in all mean field theories.

In summary, we develop a new methodology for calculating $\hat{q}$ at finite chemical potential, especially in the vicinity of CEP. Based on the QM model, $\hat{q}$ can be decomposed into the contributions from the σ and π exchange processes. A perturbative calculation up to the one-loop order indicates that both contributions almost vanish in the chiral symmetry breaking (hadronic) phase, and increase not only with temperature but also with chemical potential. In the chiral symmetry restored (QGP) phase, both contributions are approximately proportional to the parton number density as $\hat{q}_\sigma \sim (0.22 \pm 0.03) n_{\text{parton}}$, $\hat{q}_\pi \sim (0.65 \pm 0.1) n_{\text{parton}}$, thus $\hat{q} \sim (0.87 \pm 0.13) n_{\text{parton}}$. The dimensionless ratio $\hat{q}/n_{\text{parton}}$ is enhanced near the phase boundary, especially close to the first order phase boundary. We further evaluate $\hat{q}_\sigma$ in the vicinity of CEP by introducing a mapping between QCD and the Ising model, whose critical behaviors could be in the same universality class. Based on this method, we find that both the quenching parameter and the scattering rate diverge at the critical point with the scaling behavior $\hat{q} \propto SR \propto \xi^{\frac{\alpha}{\nu}}$, and the PCO, i.e., a prominent enhancement of scatterings between jet partons and medium via σ exchange, is discovered near CEP. Therefore, PCO effects on jet spectra and their substructures could serve as a novel probe of CEP, with certain advantages over the traditional ones. Our study opens a brand new perspective for improving our knowledge on the QCD phase diagram.

Notice: After accomplishing this work, we became aware of other efforts on calculating $\hat{q}$ at finite chemical potential with fairly different conclusions. [62–64]

Acknowledgements. We are grateful for valuable discussions with Abhijit Majumder, Xiaofeng Luo, Yi Yin,

Xin-Nian Wang, Shuai Y. F. Liu and Jingyi Chao. This work was supported by the National Natural Science Foundation of China (Grant Nos. 12105129, 12175122, 2021-867, and 12247101).

References

[1] Gyulassy M and McLerran L 2005 *Nucl. Phys. A* **750** 30
[2] Jacobs P and Wang X N 2005 *Prog. Part. Nucl. Phys.* **54** 443
[3] Aoki Y, Endrodi G, Fodor Z, Katz S D, and Szabo K K 2006 *Nature* **443** 675
[4] Bazavov A *et al.* 2012 *Phys. Rev. D* **85** 054503
[5] Stephanov M A 2009 *Phys. Rev. Lett.* **102** 032301
[6] Asakawa M, Ejiri S, and Kitazawa M 2009 *Phys. Rev. Lett.* **103** 262301
[7] Athanasiou C, Rajagopal K, and Stephanov M 2010 *Phys. Rev. D* **82** 074008
[8] Stephanov M A 2011 *Phys. Rev. Lett.* **107** 052301
[9] Jiang L, Li P, and Song H 2016 *Phys. Rev. C* **94** 024918
[10] Herold C, Nahrgang M, Yan Y, and Kobdaj C 2016 *Phys. Rev. C* **93** 021902
[11] Bluhm M, Nahrgang M, Bass S A, and Schaefer T 2017 *Eur. Phys. J. C* **77** 210
[12] Stephanov M and Yin Y 2018 *Phys. Rev. D* **98** 036006
[13] Wu S, Wu Z, and Song H 2019 *Phys. Rev. C* **99** 064902
[14] Nahrgang M, Bluhm M, Schaefer T, and Bass S A 2019 *Phys. Rev. D* **99** 116015
[15] An X, Başsar G, Stephanov M, and Yee H U 2020 *Phys. Rev. C* **102** 034901
[16] Pradeep M, Rajagopal K, Stephanov M, and Yin Y 2022 *Phys. Rev. D* **106** 036017
[17] Abdallah M *et al.* 2021 *Phys. Rev. C* **104** 024902
[18] Sun K J, Li F, and Ko C M 2021 *Phys. Lett. B* **816** 136258
[19] Majumder A and Van Leeuwen M 2011 *Prog. Part. Nucl. Phys.* **66** 41
[20] Armesto N, Cole B, Gale C, Horowitz W A, Jacobs P *et al.* 2012 *Phys. Rev. C* **86** 064904
[21] Bass S A *et al.* 2009 *Phys. Rev. C* **79** 024901
[22] Burke K M *et al.* 2014 *Phys. Rev. C* **90** 014909
[23] Qin G Y and Wang X N 2015 *Int. J. Mod. Phys. E* **24** 1530014
[24] Cao S S and Wang X N 2021 *Rept. Prog. Phys.* **84** 024301
[25] Chien Y T and Vitev I 2016 *J. High Energy Phys.* **2016(05)** 23
[26] Casalderrey-Solana J, Gulhan D, Milhano G, Pablos D, and Rajagopal K 2017 *J. High Energy Phys.* **2017(03)** 135
[27] Tachibana Y, Chang N B, and Qin G Y 2017 *Phys. Rev. C* **95** 044909
[28] Kunnawalkam Elayavalli R and Zapp K C 2017 *J. High Energy Phys.* **2017(07)** 141
[29] Luo T, Cao S, He Y, and Wang X N 2018 *Phys. Lett. B* **782** 707
[30] Chang N B, Cao S, and Qin G Y 2018 *Phys. Lett. B* **781** 423
[31] Mehtar-Tani Y and Tywoniuk K 2017 *J. High Energy Phys.* **2017(04)** 125
[32] Milhano G, Wiedemann U A, and Zapp K C 2018 *Phys. Lett. B* **779** 409
[33] Chen W, Cao S, Luo T, Pang L G, and Wang X N 2020 *Phys. Lett. B* **810** 135783
[34] Qin G Y, Ruppert J, Gale C, Jeon S, and Moore G D 2009 *Phys. Rev. C* **80** 054909
[35] Chen W, Cao S, Luo T, Pang L G, and Wang X N 2018 *Phys. Lett. B* **777** 86
[36] Zhang S L, Luo T, Wang X N, and Zhang B W 2018 *Phys. Rev. C* **98** 021901
[37] Chen W, Yang Z, He Y, Ke W, Pang L G, and Wang X N 2021 *Phys. Rev. Lett.* **127** 082301
[38] Chen W, Cao S S, Luo T, Pang L G, and Wang X N 2021 *Nucl. Phys. A* **1005** 121934
[39] Luo A, Mao Y X, Qin G Y, Wang E K, and Zhang H Z 2021 arXiv:2109.14314 [hep-ph]
[40] Adamczyk L *et al.* 2018 *Phys. Rev. Lett.* **121** 032301
[41] Baier R 2003 *Nucl. Phys. A* **715** 209c
[42] Majumder A 2013 *Phys. Rev. C* **80** 031902
[43] Majumder A 2013 *Phys. Rev. C* **87** 034905
[44] Panero M, Rummukainen K, and Schäfer A 2014 *Phys. Rev. Lett.* **112** 162001
[45] Kumar A, Majumder A, and Weber J H 2022 *Phys. Rev. D* **106** 034505
[46] Cao S *et al.* 2021 *Phys. Rev. C* **104** 024905
[47] Ke W Y and Wang X N 2021 *J. High Energy Phys.* **2021(05)** 041
[48] Xie M, Ke W, Zhang H Z, and Wang X N 2022 arXiv:2206.01340 [hep-ph]
[49] Schaefer B J, Pawlowski J M, and Wambach J 2007 *Phys. Rev. D* **76** 074023
[50] Parotto P, Bluhm M, Mroczek D, Nahrgang M, Noronha-Hostler J, Rajagopal K, Ratti C, Schäfer T, and Stephanov M 2020 *Phys. Rev. C* **101** 034901
[51] Martinez M, Schäfer T, and Skokov V 2019 *Phys. Rev. D* **100** 074017
[52] Kubo R 1957 *J. Phys. Soc. Jpn.* **12** 570
[53] Martin P C and Schwinger J S 1959 *Phys. Rev.* **115** 1342
[54] Onuki A 2013 *Phase Transition Dynamics* (Phase Transition Dynamics)
[55] Akamatsu Y, Teaney D, Yan F, and Yin Y 2019 *Phys. Rev. C* **100** 044901
[56] Halperin B I, Hohenberg P C, and Ma S K 1974 *Phys. Rev. B* **10** 139
[57] Zinn-Justin J 2002 *Quantum Field Theory and Critical Phenomena* (Oxford: Oxford University Press)
[58] Schweitzer D, Schlichting S, and von Smekal L 2020 *Nucl. Phys. B* **960** 115165
[59] Schweitzer D, Schlichting S, and von Smekal L 2021 arXiv:2110.01696 [hep-lat]
[60] Hohenberg P C and Halperin B I 1977 *Rev. Mod. Phys.* **49** 435
[61] Kawasaki K 1970 *Ann. Phys.* **61** 1
[62] Zhu X R and Zhang Z Q 2020 arXiv:2006.14324 [nucl-th]
[63] Grefa J, Hippert M, Noronha J, Noronha-Hostler J, Portillo I, Ratti C, and Rougemont R 2022 *Phys. Rev. D* **106** 034024
[64] McLaughlin E, Rose J, Parotto P, Ratti C, and Noronha-Hostler J 2021 arXiv:2103.03329 [nucl-th]